

The ratio of B-field and dB/dt time constants from time-domain electromagnetic data: a new tool for estimating size and conductivity of mineral deposits

Kun Guo¹ James E. Mungall^{1,3} Richard S. Smith²

¹University of Toronto, Department of Earth Sciences, 22 Russell St, Toronto, Ontario, Canada M5S 3B1.

²Laurentian University, Department of Earth Sciences, 935 Ramsay Lake Rd, Sudbury, Ontario, Canada P3E 2C6.

³Corresponding author. Email: mungall@es.utoronto.ca

Abstract. A discrete conductive sphere model in which current paths are constrained to a single planar orientation (the ‘dipping sphere’) is used to calculate the secondary response from Geotech Ltd’s VTEM airborne time domain electromagnetic (EM) system. In addition to calculating the time constants of the B-field and dB/dt responses, we focus on the time-constant ratio at a late time interval and compare numerical results with several field examples. For very strong conductors with conductivity above a critical value, both the B-field and dB/dt responses show decreasing values as the conductivity increases. Therefore response does not uniquely define conductivity. However, calculation of time constants for the decay removes the ambiguity and allows discrimination of high and low conductivity targets. A further benefit is gained by comparing the time constants of the B-field and dB/dt decays, which co-vary systematically over a wide range of target conductance. An advantage of calculating time constant ratios is that the ratios are insensitive to the dip and the depth of the targets and are stable across the conductor. Therefore we propose to use their ratio $r_\tau = \tau_B/\tau_{dB/dt}$ as a tool to estimate the size and conductivity of mineral deposits. Using the VTEM base frequency, the magnitude of r_τ reaches a limiting value of 1.32 for the most highly conductive targets. Interpretations become more complicated in the presence of conductive overburden, which appears to cause the limiting value of r_τ to increase to 2 or more.

Key words: B-field, dB/dt , decay constant, time constant ratio, time-domain EM, overburden.

Received 1 May 2013, accepted 1 August 2013, published online 12 September 2013

Introduction

Time-domain electromagnetic (TEM) systems measure the decay of a secondary field excited by the sudden removal of a primary field. The variation in time of currents induced by changes in the primary field depends on a range of parameters such as electrical conductivity, geometry of the conductor, and interaction between conductors (West and Macnae, 1991). Therefore, the secondary response generated by the induced currents can be used to interpret the physical characteristics of the conductor. At specific delay times, the decay of secondary fields, B-field and dB/dt , can be approximated by single decaying exponentials with time constant τ which is an estimate of the time over which their amplitudes drop to e^{-1} of their original values. For the B-field (Smith and Annan, 1998) and dB/dt responses we define these time constants as τ_B and $\tau_{dB/dt}$ respectively (Table 1).

The transient field inside a general layered Earth excited by the switch off of current cannot generally be written as a closed-form solution expression (Riedel et al., 2010). The methods used for computing such response generally rely heavily on numerical methods (Lamontagne, 1975; Ward and Hohmann, 1988).

Time domain EM response

Theoretical background

Following Smith and Lee (2001), we use ‘impulse response’ to refer to the secondary magnetic-field response resulting from a short pulse in the magnetic field having the delta function at zero

time removed. Asten and Duncan (2012) approximated the late-time impulse response of a conductive layered half-space with the relations

$$B(t) = -A(k-1)^{-1}t^{-(k-1)} \quad (1)$$

and

$$\frac{dB}{dt} = At^{-k}, \quad (2)$$

where $B(t)$ is the vertical component of induced magnetic field at time t , dB/dt is the time derivative of $B(t)$, A is a geometric factor, $2.5 < k < 4$. A value of $k=2.5$ corresponds to a conductive homogeneous half-space model; $k=4$ corresponds to a conductive thin layer over a resistive half-space model.

A single conductive-loop model is a simple but useful model used in EM geophysics exploration (Grant and West, 1965; Smith and Lee, 2001; Smith and West, 1988). McCracken et al. (1986) gave the time dependent responses as a decaying exponential function modified by a geometry factor G_i (also referred to as the inductive limit) and associated time constant τ of the target.

$$B(t) = -G_i \exp\left\{-\frac{t}{\tau}\right\} \quad (3)$$

and

$$\frac{dB}{dt} = \frac{G_i}{\tau} \exp\left\{-\frac{t}{\tau}\right\} \quad (4)$$

Table 1. Definitions and dimensions of geophysical quantities referred to in the text.

Symbol	Name	Unit
t	Time	s
σ	Conductivity	S/m
μ	Magnetic permeability	H/m
ε	Magnetic permittivity	F/m
a	Sphere radius	M
i	$\sqrt{-1}$	
I	Current	A
$I_m(ka)$	Bessel function of degree m	
θ	Latitudinal angle to receiver	degree
ϕ	Longitudinal angle to receiver	degree
λ_k	Zeros of $I_{1/2}$	$H^{1/2}$
$X+iY$	Frequency dependent part of the sphere response	Hz
$\Xi(t)$	Inverse Laplace transform of $X+iY$	/Hz
τ_B	Time constant of B-field	S
$\tau_{dB/dt}$	Time constant of dB/dt	S
r	Ratio of τ_B and τ	
\mathbf{B}	Magnetic flux density	T
B	z -component of \mathbf{B} -field	T
dB/dt	z -component of dB/dt	T/s
\mathbf{H}	Magnetic field strength	A/m
\mathbf{A}	Vector potential	Vs/m
\mathbf{H}_0	Primary field at the sphere	A/m
\mathbf{H}_s	Secondary field at the sphere	A/m
\mathbf{r}_{sT}	Vector from sphere to transmitter	M
\mathbf{r}_{sR}	Vector from sphere to receiver	M
\mathbf{m}_{Tx}	Dipole moment of transmitter loop	Cm
\mathbf{m}_{sph}	Dipole moment of a sphere	Cm

A real target can be approximated as the sum of an infinite number of single conductive loops. Then the impulse response would be the sum of these single conductive-loop responses and can be evaluated as

$$B(t) = - \sum G_i \exp \left\{ -\frac{t}{\tau} \right\} \quad (5)$$

and

$$\frac{dB}{dt} = \sum \frac{G_i}{\tau} \exp \left\{ -\frac{t}{\tau} \right\} \quad (6)$$

and the inductive limit response (G_T) of the target can be expressed as

$$G_T = \sum G_i \tau_i \quad (7)$$

The inductive limit response corresponds to the physical situation where the induced eddy currents only flow on the surface of the target. This happens at $t=0$ when the currents have not diffused into the target. Therefore, G_T is a purely geometric factor independent of the conductivity of the target (McCracken et al., 1986).

The following discussion is mainly based on Smith and Lee (2001). For a sphere in free space, Grant and West (1965) calculated the vector potential of a field excited by a harmonic varying field, in spherical coordinates,

$$\mathbf{A} = -\mathbf{u}_\phi \frac{\mu \sin \theta}{2r^2} a^3 H_0 (X + iY) \quad (8)$$

with frequency dependent part

$$X + iY = \frac{-3/2 I_{3/2}(ka) + ka I'_{3/2}(ka)}{3/2 I_{3/2}(ka) + ka I'_{3/2}(ka)} \quad (9)$$

where \mathbf{u}_ϕ denotes the unit vector in the longitudinal (ϕ) direction, θ is the latitude direction, H_0 is the magnitude of the primary magnetic field at the sphere, r is the distance between the receiver to the centre of the sphere; $I_{3/2}(ka)$ is the modified Bessel function of order $3/2$; the prime denotes the derivative with respect to the argument, $k = (s\mu\sigma)^{1/2}$ where s is the Laplace transform variable. The spherical polar coordinate system is oriented with the polar axis ($\theta=0$) in the direction of the primary field H_0 .

Smith and Lee (2001) simplified $X+iY$ using the second and fourth recurrence relations in equation 9.6.26 of Abramowitz and Stegun (1965) and derived

$$X + iY = \frac{I_{5/2}(ka)}{I_{1/2}(ka)} \quad (10)$$

Then the time dependent part of the impulse response can be obtained by applying an inverse Laplace transform to equation 10 (Smith and Lee, 2001),

$$\Xi(t) = - \sum_{k=0}^{\infty} \exp \left\{ \frac{-\lambda_k^2 t}{\mu\sigma a^2} \right\} \frac{6}{\mu\sigma a^2} \quad (11)$$

and

$$\int \Xi(t) dt = \sum_{k=0}^{\infty} \exp \frac{6}{\lambda_k^2} \left\{ \frac{-\lambda_k^2 t}{\mu\sigma a^2} \right\}, \quad (12)$$

where λ_k are the zeros of the modified Bessel functions of order $1/2$ ($I_{1/2}$). The modified Bessel functions has zeros of $2\pi k$, where $k=0, 1, 2, \dots$ (Smith and Wasylechko, 2012).

The primary field at the sphere \mathbf{H}_0 can be calculated using the dipole formula given by Grant and West (1965)

$$\mathbf{H}_0 = \frac{1}{4\pi r_{sT}^3} \left(\frac{3\mathbf{m}_{Tx} \cdot \mathbf{r}_{sT}}{r_{sT}^2} \mathbf{r}_{sT} - \mathbf{m}_{Tx} \right), \quad (13)$$

where \mathbf{m}_{Tx} is the transmitter dipole moment and \mathbf{r}_{sT} is the vector from the sphere to the transmitter. This formula adopts a Cartesian coordinate system with the origin at the centre of the transmitter. The secondary magnetic field at the receiver \mathbf{H}_s can be calculated by setting \mathbf{r}_{sR} as the offset vector from the receiver to the sphere and \mathbf{m}_{sph} as the moment of the sphere.

$$\mathbf{H}_s = \frac{1}{4\pi r_{sR}^3} \left(\frac{3\mathbf{m}_{sph} \cdot \mathbf{r}_{sR}}{r_{sR}^2} \mathbf{r}_{sR} - \mathbf{m}_{sph} \right) \quad (14)$$

Modelling the B-field and dB/dt responses

This study focuses on the z -component of both dB/dt and B-field responses for a system configured to resemble Geotech's VTEM system, which adopts a superimposed coplanar dipole configuration. The outer-most transmitter loop has four turns of the transmitter wires with vertical (z , perpendicular to the ground) axis. One of the wires is extended and wrapped in the bucking coil in between the transmitter loop and receiver in the centre (Kuzmin and Morrison, 2008). The system takes dB/dt measurement as a direct measurement of the electromotive force (EMF) induced in the receiver coil during both on- and off-time. The B-field response can be obtained through numerical integration of the entire on-time and off-time secondary response (Smith and Annan, 2000). However, only off-time data are reported because of the inherently noisy character of the on-time data.

The numerical data used in this study are generated by a conductive sphere model (Smith and Lee, 2001). The EM responses are calculated by convolving equations 11 and 12

with the VTEM waveform (Figure 1). The model can also be used to model plate-like bodies by constraining the current to flow in a specific dipping plane (Smith and Lee, 2001; Smith and Wasylechko, 2012). Although thin sheet conductor geometries are commonly encountered in field situations we have retained the ‘dipping sphere’ model in the present contribution because of its greater computational tractability and its generality in representing both planar and solid body geometries. In future work, we intend also to explore the responses of thin sheet conductor geometries, including more complex systems involving multiple interacting sheets.

As Figure 2 shows, B-field and dB/dt both resemble exponentially decaying functions because both are series of decaying exponentials. At early time, the decay curves have almost identical slopes; however, at later off-time, dB/dt has a larger negative slope and decays faster. The amplitude factor in front of each exponential in equations 11 and 12 is different and, as a result, the relative importance of each exponential in the sum changes. Hence integration from dB/dt to B-field will put emphasis on a different exponential with a different time constant. At a specific delay time, the resulting decay curves can be approximated as single exponential functions each with a single characteristic time constant by taking their slopes if we approximate the responses as

$$B(t) = A \exp \left\{ -\frac{t}{\tau_B} \right\}, \quad (15)$$

and

$$\frac{dB}{dt}(t) = B \exp \left\{ -\frac{t}{\tau_{dB/dt}} \right\} \quad (16)$$

where A and B are arbitrary constants. However, because the responses are summed over many exponential functions each having a different time constant, τ is not a constant but instead varies with time.

The time constants at a certain off-time $\tau_B, \tau_{dB/dt}$ can be calculated by linear regression over a short time interval of the decay as

$$\tau_B = -\frac{N \sum_{i=1}^N t_i^2 - \left(\sum_{i=1}^N t_i \right)^2}{N \sum_{i=1}^N t_i \ln B(t_i) - \sum_{i=1}^N t_i \sum_{i=1}^N \ln B(t_i)} \quad (17)$$

$$\tau_{dB/dt} = -\frac{N \sum_{i=1}^N t_i^2 - \left(\sum_{i=1}^N t_i \right)^2}{N \sum_{i=1}^N t_i \ln \frac{dB}{dt}(t_i) - \sum_{i=1}^N t_i \sum_{i=1}^N \ln \frac{dB}{dt}(t_i)} \quad (18)$$

and we define their ratio r_τ as

$$r_\tau = \frac{\tau_B}{\tau_{dB/dt}} \quad (19)$$

where the t_i are off-time and, N is the number of time gates.

Figure 3 shows nomograms for the dB/dt and B-field responses of 33 time gates, each of which appears as a different curve of response versus target conductivity. The amplitude of the off-time responses peaks at progressively higher conductivities as we progress from early to late time gates. For conductors with higher conductivity than the peak response, the responses fall off, tending to decay at the same rate and converge at high conductivity. A simple visual assessment of the response amplitude on a flight line profile, therefore, does not allow a unique interpretation of the target conductivity. Both B-field and dB/dt responses at the latest time gates are well above the noise floor for the conductor parameters chosen in this example.

Figure 4 shows that the time constants of B-field and dB/dt remain almost the same at low conductivities and begin to diverge as the conductivity of the sphere increases. Whereas $\tau_{dB/dt}$ tends to level off at conductivity greater than 10^3 S/m, the τ_B continues to increase. We therefore have calculated the ratio r_τ to assess its merit as a single-valued measure of the strength of a conductive target.

The values of r_τ in Figure 5 are numerical results calculated from the last two time gates for spheres with radius ranging from 25 m to 100 m at the same depth (150 m). The ratios generally rise from a value of 1 at low conductivity and converge to a value of 1.32 at conductivity of 100,000 S/m. For spheres of larger size, the ratio begins transition from 1 to 1.32 at smaller conductivities. For a sphere of radius 25 m, the ratio r_τ remains at 1 until the conductivity of the sphere reaches 100 S/m; while for a sphere of radius 100 m, the ratio r_τ tends to rise above one at conductivity of 20 S/m.

The value of r_τ for spheres of the same radius at different depths was also calculated and it was found that it does not depend on depth. It was also found not to vary with different directions in which induced currents flow, suggesting independence of r_τ to dip of conductive targets.

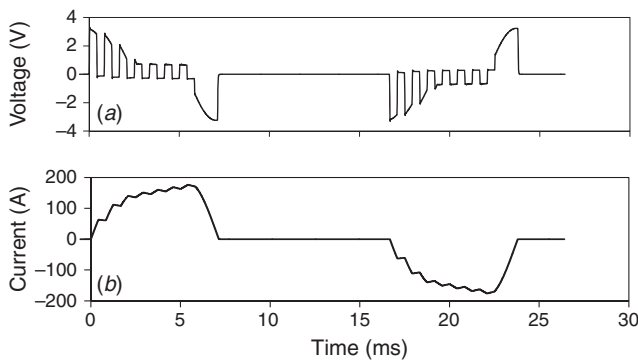


Fig. 1. Waveform of VTEM system used in this study (Fiset et al., 2010). (a) Voltage versus time over one complete duty cycle. (b) Current versus time.

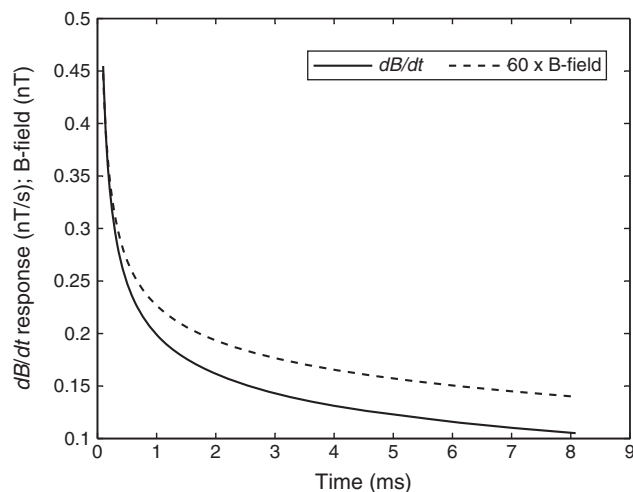


Fig. 2. B-field and dB/dt decay curves modelled using a sphere of 50 m radius with conductivity of 100 S/m at 150 m depth. B-field response shown is in units of nT multiplied by 60 to put in scale with dB/dt ; dB/dt response is in units of nT/s.

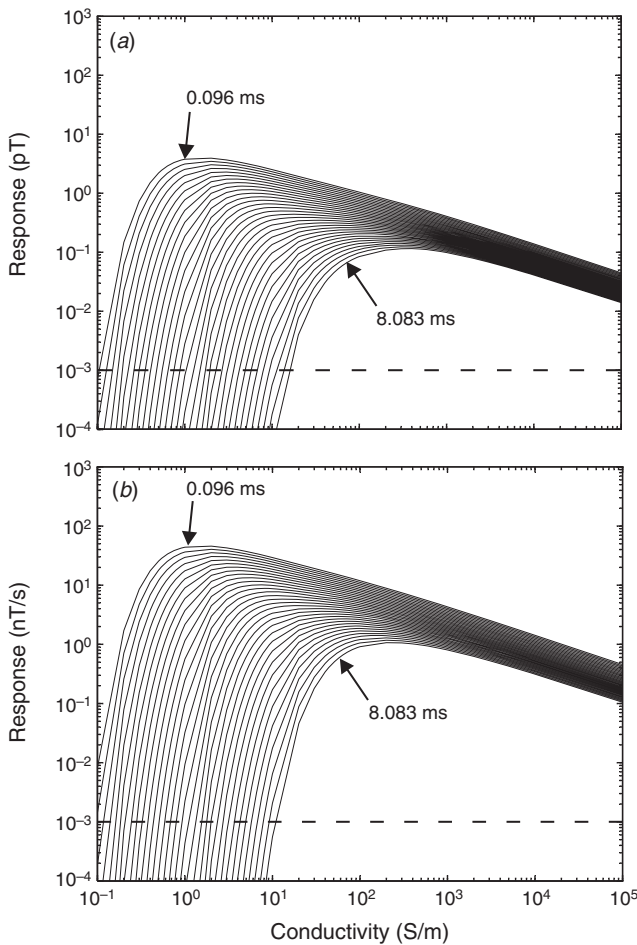


Fig. 3. Nomograms calculated for VTEM system: (a) off-time B-field and (b) off-time dB/dt . Model generated using a sphere of 50 m radius at 150 m depth. System noise floors (0.001 pT for B-field and 0.001 nT/s for dB/dt) are indicated by the dotted lines.

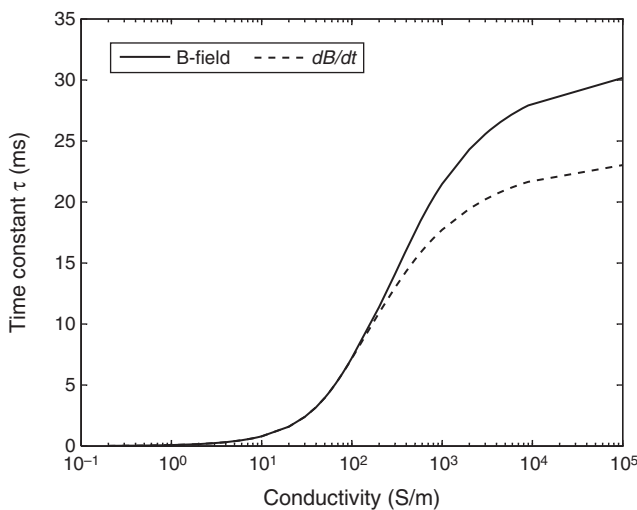


Fig. 4. Calculated time constants of B-field and dB/dt over a range of conductivities using a sphere of radius 50 m at 150 m depth. The time constants were calculated from the last two time gates (7.036 ms–8.083 ms) with equations 17 and 18.

Field examples

In order to validate the modelling results, we examine the results of several VTEM surveys chosen to represent the cases of both

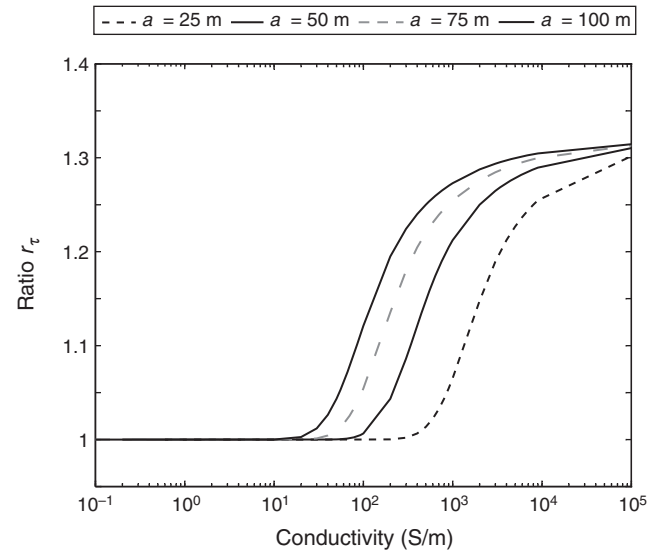


Fig. 5. Ratio r_τ generated with spheres of different radius at depth of 150 m.

weak and strong conductors lacking significant overburden as well as a strong bedrock conductor underlying a thick conductive overburden. The first example was flown by Geotech Ltd in cooperation with Noront Resources Ltd over a block located ~58 km north-west of Sudbury, Ontario, and the data were donated to the University of Toronto. Flight lines were oriented on an azimuth of 0° with a traverse line spacing of 100 m. The helicopter was maintained at a mean height of 75 m above the ground with a nominal survey speed of 80 km/h. This allowed for a nominal EM sensor terrain clearance of 40 m. The data were recorded every 0.1 s or every 2.2 m along flight track. The transmitter coil had a diameter of 25.5 m with effective coil area 508 m^2 . The system was operated at base frequency of 30 Hz with a peak current of 184 A giving a peak dipole moment of $375,878 \text{ Am}^2$. The current impulse width was 7.16 ms and the duty cycle 43%. A significant anomaly occurs along profile L1130 (Figure 6) and time constants τ_B and $\tau_{dB/dt}$ over the main anomaly are calculated using equations 17 and 18 at time gates 6.125 ms and 7.036 ms (Figures 7, 8).

As the transmitter–receiver moves towards the anomaly region, the time constants and their ratio r_τ change from noisy to stable, appearing as a plateau at ~5182400 N. Then they become noisy again as the transmitter–receiver moves away from anomaly region.

Diamond drilling and trenching by Falconbridge Limited in 1988 (Gray, 1989) intersected massive pyrrhotite sheets a few centimetres in width, hosted by chert and carbonate in a succession of tuff and clastic sediments. The sequence and the conductive sulphide horizon are well exposed in exploration trenches at the top of a hill. There is dry, well drained sandy overburden with a negligible thickness of ~1.3 m. The significant drop in time constants and their ratio at ~5182470 N is where the VTEM survey line crosses the top of the dipping pyrrhotite sheets. This is where minimum current coupling occurs and thus minimum secondary field is generated. This minimum can result in erratic behaviour when taking ratios. Over the main anomaly, the average of τ_B is 5.73 ± 1.05 and the average of $\tau_{dB/dt}$ is 4.47 ± 0.53 ; the average of r_τ is 1.28 ± 0.19 .

From Figure 8 and the standard deviations calculated above, we can see that whereas time constants τ_B and $\tau_{dB/dt}$ are quite variable over the dipping conductive sheet, the ratio r_τ is much more stable. The average of r_τ lies in the range of 1.00 to 1.32 as depicted in Figure 5. According to Pearce et al. (2006), the

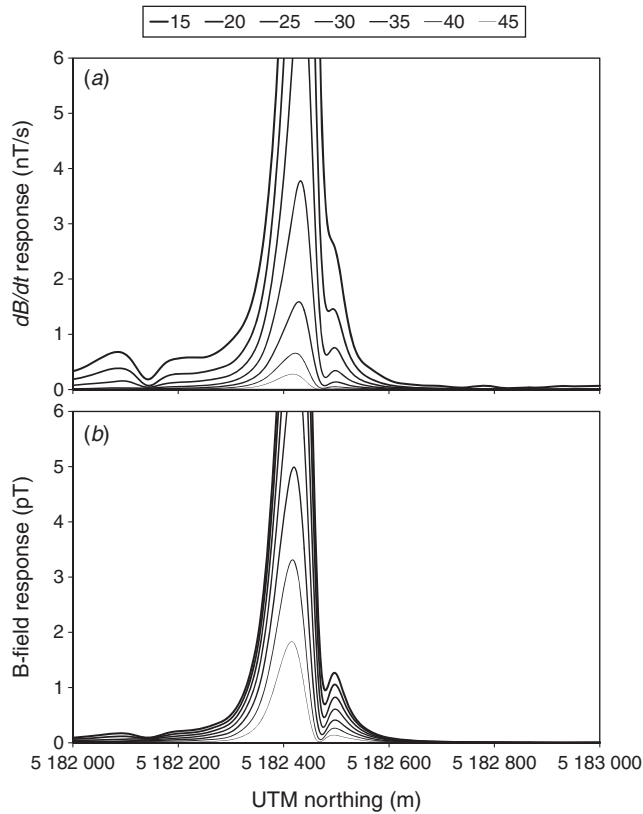


Fig. 6. (a) dB/dt response and (b) B-field response along profile L1130 for selected time gates identified with different line weights as shown in the legend insert. The horizontal axis is the UTM northing in metres. Windows 14 to 45 are recorded after the transmitter is turned off. The windows times for time gates 14 to 45 are listed in an Excel file available on the Journal’s website. The response geometry suggests that the target is a thin sheet that dips steeply to the south.

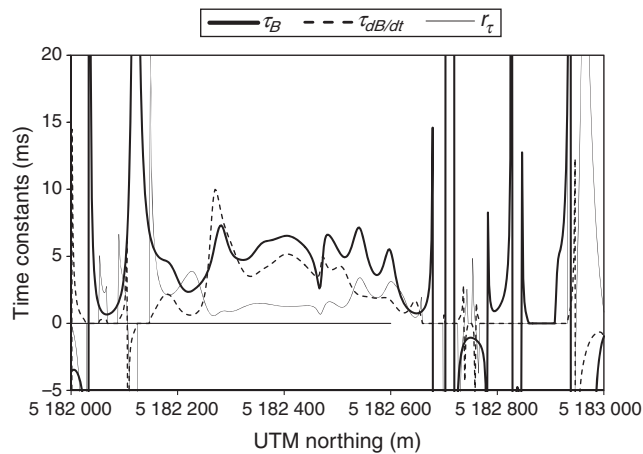


Fig. 7. Time constants and time constants ratio along profile L1130.

measured conductivity of pyrrhotite ranges from 10^3 to 10^5 S/m. With reference to Figure 6, we can estimate that the conductive sheet has a response similar to that of a conductive sphere smaller than 150 m in diameter.

Another field example is from a survey conducted by Geotech Ltd over Bold Venture’s Lizar property in the north-western Ontario over intercalated sulphide-rich metasediments and volcanic rocks. The flight specifications are the same as the field example above. Profile L2290, presented in Figure 9, was flown on a 0° azimuth.

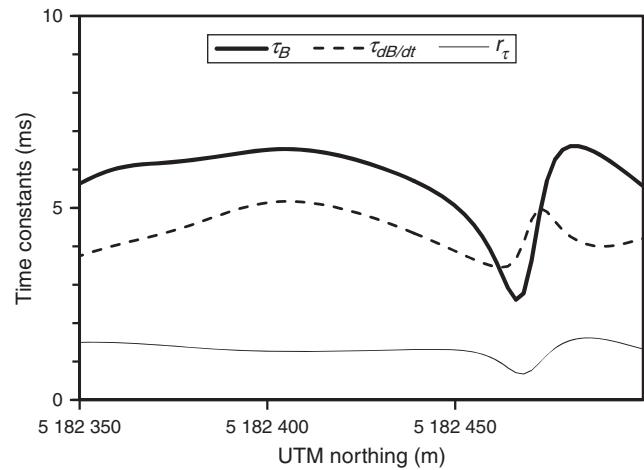


Fig. 8. Time constants and time constants ratio over the main anomaly on L1130.

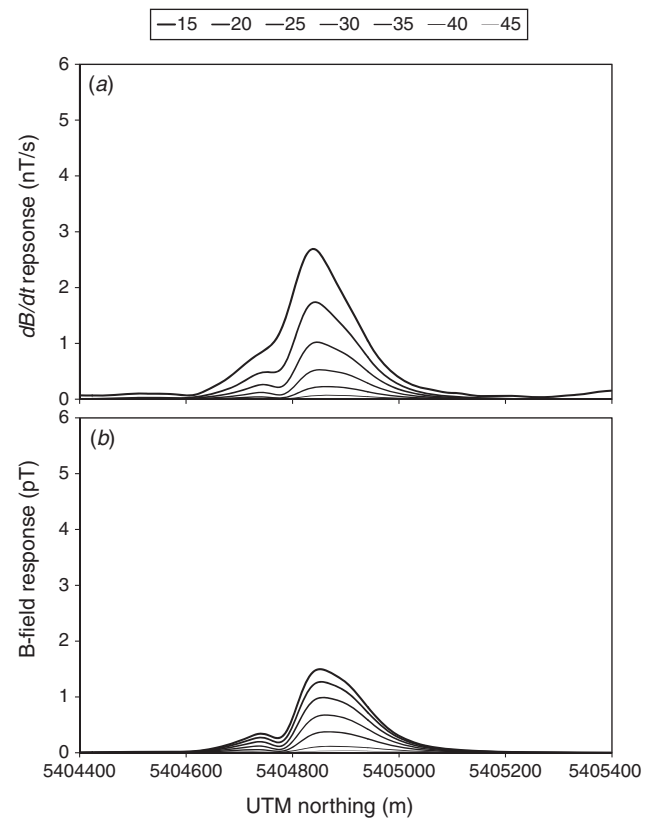


Fig. 9. Profile L2290 of Lizar VTEM survey. (a) dB/dt response and (b) B-field response (z -direction) for selected time gates identified with different line weights as shown in the legend insert. Time gates 14 to 45 were recorded. The horizontal axis is the UTM northing in metres.

Over the main anomaly, which has a much lower amplitude response than the previous example, the average of τ_B is 2.85 ± 0.4 ; the average of $\tau_{dB/dt}$ is 2.56 ± 0.34 and the average r_τ is 1.12 ± 0.12 (Figure 10). For this anomaly, both time constants are smaller compared with the previous example, which indicates low conductivity of the target and is confirmed by the ratio r_τ , which is close to 1.00.

A third field example is from a VTEM survey over a boggy area underlain by a sulphide-facies iron formation 135 km north-east of Webequie, Ontario, Canada, on an exploration property called Area 53 belonging to Bold Ventures Ltd. Flight lines were

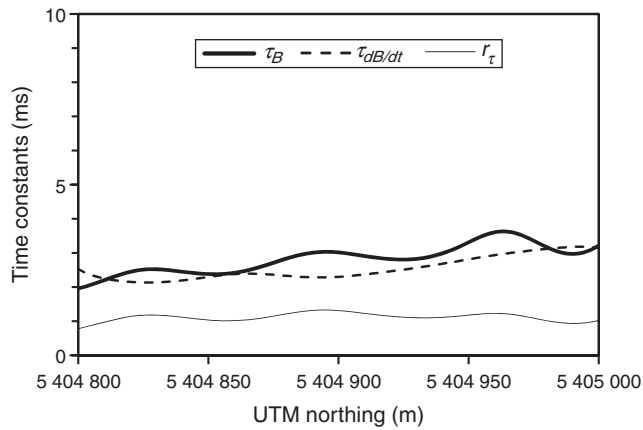


Fig. 10. Time constants and time constants ratio over the main anomaly on L2290, Lizar VTEM survey, calculated from the latest time gates. Horizontal scale is as in Figure 9.

oriented on an azimuth of 43.2° with a traverse line spacing of 200 m. The helicopter was maintained at a mean altitude of 73 m above the ground at nominal speed of 80 km/h, which allowed a nominal EM bird terrain clearance of 38 m. All loops were towed at a mean distance of 35 m below the aircraft. The data was recorded every 0.1 s or every 2.2 m along flight track. The transmitter coil has a diameter of 26 m. The system was operated at base frequency of 30 Hz with a peak current of 178 A, giving peak dipole moment $377,829 \text{ Am}^2$. The current waveform pulse width was 7.16 ms, and the duty cycle 42%. Time gates 14 to 46 were recorded.

The high early-time response even far away from the main anomaly shown in Figure 11 indicates the presence of conductive overburden (note that the first channel is only visible in the top right corner of Figure 11a). Diamond drilling has confirmed the overburden to be water-saturated clay, sand and gravel with a thickness of ~ 43 m, overlain by at least 1 m of peat. A zone of iron formation ~ 50 m in true thickness, centred on and dipping sub-vertically below the conductor axis, contains abundant well connected pyrrhotite laminae and beds up to 0.5 m thick. Over the main anomaly, the average of τ_B is 9.8 ± 1.21 and the average of $\tau_{dB/dt}$ is 4.09 ± 0.41 . The value of r_τ for this target (Figure 12) far exceeds the limit of 1.32 that was established from modelling.

Discussion

The time constant ratio r_τ is mainly dependent on conductivity and size of the targets. It remains at 1.00 at low conductivities, rises above 1.00 and diverges at higher conductivities depending on the radius. At very high conductivities above 10^5 S/m , r_τ converges to a constant value of 1.32 in the absence of conductive overburden. Preliminary modelling indicates that changing the base frequency changes the value of the asymptote but not the fundamental behaviour of r_τ . Despite the sensitivity of τ_B , $\tau_{dB/dt}$ to geometry and depth of conductive targets, the value of r_τ remains stable across the target and is independent of conductor depth. Therefore we can use r_τ as a tool to estimate the size or conductivity of the target. If the line spacing between survey lines is fine enough, we can estimate the size of the target and then estimate the conductivity. Vice versa, we can estimate the size of the target by knowing the conductivity without the line spacing.

An important limitation of r_τ is observed for highly conductive bodies both in the field and in the model. The ratio converges on a limiting value of 1.32 for bodies of all sizes with conductivities beyond 10^5 S/m such that the sizes and conductivities of various targets cannot be distinguished. For extremely conductive targets,

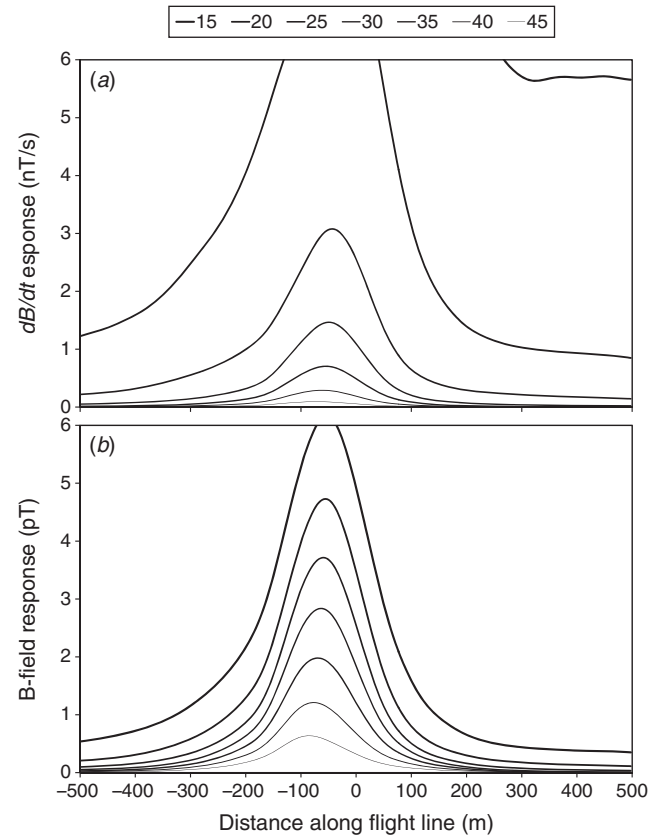


Fig. 11. (a) dB/dt response and (b) B-field response over the anomaly area along L3130, in Area 53. Horizontal scale is in metres along the flight line measured relative to an arbitrarily chosen point at the centre of the anomaly in the first time gate.

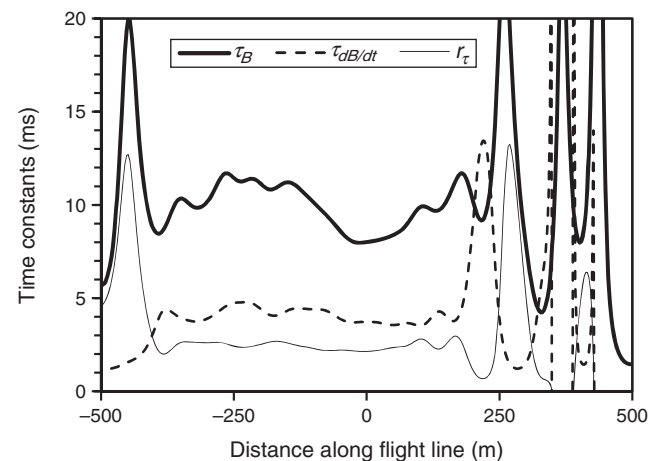


Fig. 12. Time constants and time constants ratio over the main anomaly on L3130 calculated on the latest time gates, Area 53. Horizontal scale is as in Figure 11.

any induced currents would reside on the surface of the target and the decay of the B-field and dB/dt responses would be below the noise level and would not be detected at all. Since this limiting value of r_τ is attained even for thin broad sheets of pyrrhotite a few centimetres thick, it would be desirable to find a way to extend the range of conductivity over which responses continue to vary with conductivity. Ways to increase airborne TDEM systems' sensitivity to extremely conductive bodies might include direct on-time measurement or the use of a lengthened duty cycle with

longer off-time measurements combined with improved signal to noise ratios.

Additional problems arise with the presence of conductive overburden as the overburden will also produce a secondary response and may conceal or interact with the response from any conductive ore body that may be present (Hurley, 1977). Hurley gave the approximate solution for response from low conductivity overburden. The present work suggests that r_{τ} is strongly enhanced by interaction of the overburden with the bedrock conductor but we have not been able to model this as of yet. Future work could be done by combining the overburden response with sphere response and calculating r_{τ} with the presence of overburden at different conductivities and thickness.

Although the target at Area 53 was composed of barren metasedimentary pyrrhotite, the total amount of sulphide present, its geometric form, and its geophysical response are very similar to that of the Eagle's Nest Ni–Cu–Pt massive sulphide deposit ~50 km to the south-west (fig. 10 in Balch et al., 2010). In the case of the Eagle's Nest deposit there is also conductive overburden, with somewhat lower early-time responses than in the present location, and there too the r_{τ} can be estimated from published data to be ~2.00, greatly exceeding the model limit of 1.32.

Acknowledgements

We thank Geotech Ltd, Noront Resources Ltd and Bold Ventures Ltd for permission to investigate and present VTEM data; Noront Resources Ltd and Geotech Ltd are especially thanked for their generosity in paying for the VTEM survey presented in Figures 6–8, which was donated to the University of Toronto in 2010.

References

- Abramowitz, M., and Stegun, I. A., 1965, *Handbook of mathematical functions with formulas, graphs, and mathematical tables*: US Government Print Off.
- Asten, M. W., and Duncan, A. W., 2012, The quantitative advantage of using B-field sensors in time-domain EM measurement for mineral exploration and unexploded ordnance search: *Geophysics*, **77**, WB137–WB148. doi:10.1190/geo2011-0385.1
- Balch, S. J., Mungall, J. E., and Niemi, J., 2010, Present and future geophysical methods for Ni-Cu-PGE exploration: lessons from McFaulds Lake, Northern Ontario: SEG Special Publication **15**, 559–572.
- Fiset, N., Acom, W., Legault, J., and Smith, G., 2010, Report on a helicopter-borne versatile time-domain electromagnetic (VTEM) and aeromagnetic geophysical survey: Geotech Ltd, Project 10034.
- Grant, F. S., and West, G. F., 1965, *Interpretation theory in applied geophysics*: McGraw Hill.
- Gray, M. J., 1989, 1988 Diamond Drill Programme Assessment Report - TH Option - Cartier Area: Ontario Ministry of Northern Development and Mines Assessment Report 41112NE0064 16.
- Hurley, D. G., 1977, The effect of a conductive overburden on the transient electromagnetic response of a sphere: *Geoexploration*, **15**, 77–85. doi:10.1016/0016-7142(77)90014-X
- Kuzmin, P. V., and Morrison, E. B., 2008, Bucking coil and B-field measurement and apparatus for time domain electromagnetic measurements: United States patent application publication No. US2010/0052685 A1.
- Lamontagne, Y., 1975, Applications of wideband, time domain, EM measurements in mineral exploration: Ph.D. thesis, University of Toronto
- McCracken, K. G., Oritaglio, M. L., and Hohmann, G. W., 1986, A comparison of electromagnetic exploration systems: *Geophysics*, **51**, 810–818. doi:10.1190/1.1442133
- Pearce, C. I., Patrick, R. A. D., and Vaughan, D. J., 2006, Electrical and magnetic properties of sulphides: *Reviews in Mineralogy and Geochemistry*, **61**, 127–180. doi:10.2138/rmg.2006.61.3
- Riedel, M., Willoughby E. C., and Chopra, S., 2010, Gas hydrates geophysical exploration techniques and methods, in M. Riedel, E. C. Willoughby, and S. Chopra, eds., *Geophysical Characterization of Gas Hydrates*: SEG Geophysical Development Series, **14**, 1–22.
- Smith, R. S., and Annan, A. P., 1998, The use of B-field measurement in an airborne time-domain system: Part I. Benefits of B-field versus dB/dt: *Exploration Geophysics*, **29**, 24–29. doi:10.1071/EG998024
- Smith, R. S., and Annan, A. P., 2000, Using an induction coil sensor to indirectly measure the B-field response in the bandwidth of the transient electromagnetic method: *Geophysics*, **65**, 1489–1494. doi:10.1190/1.1444837
- Smith, R. S., and Lee, T. J., 2001, The impulse-response moments of a conductive sphere in a uniform field, a versatile and efficient electromagnetic model: *Exploration Geophysics*, **32**, 113–118. doi:10.1071/EG01113
- Smith, R. S., and Wasylechko, R., 2012, Sensitivity cross-sections in airborne electromagnetic methods using discrete conductors: *Exploration Geophysics*, **43**, 95–103. doi:10.1071/EG11048
- Smith, R. S., and West, G. F., 1988, Inductive interaction between polarizable conductors: an explanation of a negative coincident-loop transient electromagnetic response: *Geophysics*, **53**, 677–690. doi:10.1190/1.1442502
- Ward, S. H., and Hohmann, G. W. 1988, Electromagnetic theory for geophysical applications, in M. N. Nabighian, ed., *Electromagnetic methods in applied geophysics*: SEG Special Volume **2**, 131–311.
- West, G. F., and Macnae, J. C., 1991, Physics of the electromagnetic induction exploration method, in M. N. Nabighian, ed., *Electromagnetic methods in applied geophysics*: SEG Special Volume **2**, Part A, 1–45.